Molina Puerto, J.; Fernández Sáez, J.; García Albert, C.; Del Río García, AI.; Bonastre Cano, JA.; Cases Iborra, FJ. (2015). Electrochemical characterization of electrochemically reduced graphene coatings on platinum. Electrochemical study of dye adsorption. Electrochimica Acta. 166:54-63. doi:10.1016/j.electacta.2015.03.054.

Electrochemical characterization of electrochemically reduced graphene coatings on platinum. Electrochemical study of dye adsorption.

J. Molina[a], J. Fernández[a], C. García[a], A.I. del Río[a], J. Bonastre[a], F. Cases[a,1]*

[a]*Departamento de Ingeniería Textil y Papelera, EPS de Alcoy, Universitat Politècnica de València, Plaza Ferrándiz y Carbonell s/n, 03801 Alcoy, Spain*

Abstract

Reduced graphene oxide coatings were synthesized by cyclic voltammetry on Pt electrodes. Electrochemically reduced graphene oxide was analyzed by scanning electrochemical microscopy for the first time. The redox mediator influences the electrochemical response; thus $Ru(NH_3)_6^{3+}$ and $Fe(CN)_6^{3-}$ gave a similar response and Fe^{3+} gave the poorest response. Pt electrodes coated with reduced graphene oxide were also used in the electrochemical adsorption (performed by cyclic voltammetry) of different dyes (Methylene Blue, Procion MX-2R and Amaranth). Electrochemical methods proved to be useful to monitor the adsorption of dyes on the surface of graphene materials. After adsorption, with Methylene Blue and Procion MX-2R, the appearance of a stable redox pair (with 1 electron transfer) was observed. This redox pair was adsorption controlled since the intensity of the redox pair was proportional to the scan rate used. Electrochemical adsorption multiplied by 3 the electrical charge of the Methylene Blue adsorbed on the surface of reduced graphene oxide when compared with simple adsorption at open circuit potential. In the case of Procion MX-2R, the increase obtained was even higher, with a 6-fold increase.

Keywords: graphene, reduced graphene oxide, scanning electrochemical microscopy, dye, adsorption.

---

* Corresponding author. Fax.: +34 966528438; telephone: +34 966528412.

[1] ISE member

E-mail addresses: jamopue@doctor.upv.es (J. Molina), jaferse1@posgrado.upv.es (J. Fernández), cagaral@epsa.upv.es (C. García), delgaran@doctor.upv.es (A. I. del Río), joboca@txp.upv.es (J. Bonastre), fjcases@txp.upv.es (F. Cases).

1. Introduction

Since the discovery of graphene by Novoselov et al. [1], graphene has emerged as a revolutionary material in the field of physics and materials science due to its electronic [2], optical [3], thermal [4] and mechanical properties [5,6]. Different methods of production have been used for the production of graphene and derivatives [7,8]. High quality graphene crystals are obtained from mechanical exfoliation (the first method reported by Novoselov et al.) [1], however its production is limited to low quantities only useful for basic studies. This is why other methods with higher production capacity have been used, for instance: chemical vapour deposition [7,8] or chemical methods [7-9]. Among chemical methods, the production of graphene oxide (GO) is of particular interest due to the low production costs and its versatility. The reduction of GO allows the deposition of reduced graphene oxide (RGO) on different substrates. The reduction can be performed thermally, photocatalytically, chemically, electrochemically, etc. [10]. Electrochemical reduction is of particular interest because its ease of operation and control, and no additional reagents such as dangerous reductants (for instance

hydrazine) are needed [10]. The applications of graphene and derivatives in chemistry and electrochemistry are varied and numerous and include energy storage [7], sensors [7], oxygen reduction reaction [11] or photocatalysis [12] among others.

Scanning electrochemical microscopy (SECM) is a powerful technique that has been used to test the electroactivity of samples ranging from biological applications [13] to materials characterization such as corrosion processes [14]. Some studies have focused on the electrochemical characterization of graphene, graphene oxide and reduced graphene oxide by SECM [15-21]. However, the characterization by SECM of RGO obtained by electrochemical methods has not been reported in bibliography. This is the reason why electrochemical characterization by SECM of RGO deposited on Pt electrochemically was performed in this paper.

The interaction of graphene with organic molecules has been shown to be of interest; for instance the doping (n or p) of graphene with aromatic molecules has been demonstrated [22]. Graphene and derivatives have also been shown to be good adsorbents for dyes due to the π-π stacking interaction between graphene and aromatic compounds [23,24]. These materials could have applications in dye-sensitized biosensors [25] or charge transfer complexes [26-28]. In this paper, the electrochemical adsorption of different dyes by cyclic voltammetry (CV) is proposed as a method to monitor the adsorption of the dye and a more efficient way of adsorbing dyes than open circuit adsorption. The RGO/dye complexes were also later characterized by CV in order to evaluate the adsorption products as well as its electrochemical properties.

2. Experimental

2.1. Reagents and materials

All reagents used were of analytical grade.

For the synthesis: Monolayer graphene oxide (GO) powders were acquired from Nanoinnova Technologies S.L. (Spain). Lithium perchlorate ($LiClO_4$) was purchased from Merck. Pt wires (0.5 mm diameter, 99.99% purity) were acquired from Engelhard-Clal. The effective length of the electrodes used (where reaction occurred) was 2 cm (total area of 0.31 cm^2). The area of the electrodes was controlled with Teflon®.

For the characterization: Sulphuric acid (H_2SO_4) and potassium chloride (KCl) were purchased from Merck. Hexaammineruthenium (III) chloride ($Ru(NH_3)_6Cl_3$), potassium ferrocyanide (III) $K_3Fe(CN)_6$ and iron (III) sulfate pentahydrate ($Fe_2(SO_4)_3 \cdot 5H_2O$) were used as received from Acrōs Organics. Methylene Blue (MB), Procion MX-2R (PMX2R) and Amaranth (AM) were purchased from Panreac, Zeneca and Fluka, respectively.

When needed, solutions were deoxygenated by bubbling nitrogen (N_2 premier X50S). Ultrapure water was obtained from an Elix 3 Millipore-Milli-Q Advantage A10 system with a resistivity near to 18.2 MΩ cm.

2.2. Synthesis of reduced graphene oxide on Pt

An Autolab PGSTAT302 potentiostat/galvanostat was used to perform cyclic voltammetry (CV) as well as electrochemical impedance spectroscopy (EIS) measurements. GO was reduced on the surface of Pt by CV. The solution used for the synthesis contained ultrapure water, 3 g L^{-1} GO and 0.1 M $LiClO_4$ (supporting electrolyte). Pt electrodes were pretreated with a flame treatment to clean their surface [29]. A three-electrode configuration was used for the synthesis: a Pt wire was used as counter electrode and Ag/AgCl (3.5 M KCl) was used as reference electrode. To

perform the electrochemical synthesis, the potential was cycled between +0.6 V and -1.4 V at 50 mV s^{-1} for 40 scans.

2.3. Field emission scanning electron microscopy (FESEM)

A Zeiss Ultra 55 FESEM was used to observe the morphology of the samples, using an acceleration voltage of 3 kV. Energy dispersive X-ray (EDX) measurements were performed between 0 and 10 kV.

2.4. Electrochemical characterization by cyclic voltammetry (CV)

After synthesis, the electrodes were characterized by CV in 0.5 M H_2SO_4 to test their characteristic capacitive behavior. Electrodes were also tested with different redox systems (0.01 M $Ru(NH_3)_6^{3+}$ / 0.1 KCl; 0.01 M $Fe(CN)_6^{3-}$ / 0.1 M KCl and 0.02 M Fe^{3+} / 0.5 M H_2SO_4) to test their reversibility and therefore the electrochemical behavior of the electrode surface.

2.5. Electrochemical impedance spectroscopy (EIS)

The same configuration used for the synthesis of RGO on Pt was used for the EIS characterization of the electrodes in 0.5 M H_2SO_4 solution.

The experimental results were also fitted using a non-linear least squares fitting minimization method by ZView software (version 2.7).

2.6. Scanning electrochemical microscopy (SECM)

SECM measurements were carried out with a scanning electrochemical microscope of Sensolytics. A three-electrode configuration cell consisting of a 25-μm-diameter Pt microelectrode, a Pt wire auxiliary electrode and Ag/AgCl (3.5 M KCl) reference

electrode. Measurements were performed with the same redox systems used in the CV characterization: 0.01 M $Ru(NH_3)_6^{3+}$ / 0.1 KCl; 0.01 M $Fe(CN)_6^{3-}$ / 0.1 M KCl and 0.02 M Fe^{3+} / 0.5 M H_2SO_4. All the experiments were carried out in an inert nitrogen atmosphere.

The samples were glued to microscope slides with epoxy resin. The microelectrode operated at a potential of -0.4 V, 0 V, -0.1 V for the 0.01 M $Ru(NH_3)_6^{3+}$ / 0.1 KCl, 0.01 M $Fe(CN)_6^{3-}$ / 0.1 M KCl and 0.02 M Fe^{3+} / 0.5 M H_2SO_4 systems, respectively. At these potentials, the oxidized form of the redox mediator (Ox) is reduced (Red) at a diffusion controlled rate. Approach curves were obtained by recording the tip reduction current as the microelectrode tip was moved in z direction (approaching the sample). Approach curves give us an indication of the surface's electroactivity. These curves were compared to the theoretical ones (positive and negative feedback models). The substrate's surface in all the measurements was at their ocp.

2.7. Electrochemical behavior of dyes on the surface of Pt/RGO electrodes

The electrochemical behavior of different dyes was tested by means of CV. Solutions containing $5 \cdot 10^{-3}$ M of MB, PMX2R and AM and 0.5 M H_2SO_4 were used for this purpose. A three-electrode configuration was used. Potential was cycled between -0.2 V and +0.7 V for 100 scans to produce the adsorption of the dyes. An experiment was also performed at ocp in the same conditions to evaluate the spontaneous adsorption of dyes during 1 hour. The potential evolution during ocp adsorption was monitored by means of chronopotentiometry (zero current). The electrodes were characterized previously and after dyes' adsorption in 0.5 M H_2SO_4 solutions to determine possible adsorption products on the surface of RGO. To evaluate dye adsorption, the electrodes were rinsed with water several times in order to eliminate the dye not adsorbed. The electrodes were

also characterized at different scan rates to determine if the processes were diffusion or adsorption controlled and determine the number of electrons involved.

3. Results and discussion

3.1. Field emission scanning electron microscopy (FESEM)

Fig. 1 shows the FESEM micrographs and EDX analysis of the Pt/RGO electrode obtained by means of cyclic voltammetry, sweeping the potential from +0.6 V to -1.4 V for 40 scans. The whole surface of the Pt electrode was coated by RGO sheets; in Fig. 1-a RGO sheets deposited on Pt have been magnified for better observation. EDX was used to analyze chemically the composition of the sample (Fig. 1-b). C, O and Pt appeared in the spectrum; C and O arise from GO. The presence of Pt is due to the penetration of the X-ray that is in the order of μm, much higher than the thickness of the coating. The O/C atomic ratio obtained was 0.08, which indicates a high reduction of the GO sheets when compared with other methods [10].

3.2. Cyclic voltammetry and electrochemical impedance spectroscopy characterization

Fig. 2-a shows the voltammetric characterization of Pt and Pt/RGO electrodes in 0.5 M H_2SO_4 solution. As can be seen, the deposition of RGO on Pt inhibits the appearance of the characteristic oxidation and reduction processes on the platinum surface. The voltammetric profile shows the characteristic capacitive behavior of RGO. The oxidation/reduction peaks that appear between +0.2 V and +0.5 V have been attributed to a redox pair of oxygen containing groups [30,31] that are too stable to be reduced by

cyclic voltammetry [30]. The electrochemical reduction is not capable of eliminating completely the oxidized functional groups and C-OH, C=O and C-O-C groups are still present after electrochemical reduction [32]. However the O/C ratio obtained by electrochemical method is lower than the one achieved by chemical reduction methods [21], which implies that a more efficient reduction of GO is achieved by electrochemical methods.

Fig. 2-b shows the voltammetric characterization of Pt/RGO electrodes with different redox mediators ($Fe(CN)_6^{3-}$, $Ru(NH_3)_6^{3+}$ and Fe^{3+}). The peak to peak potential separation for the different redox mediators was 101, 121 and 538 mV for $Ru(NH_3)_6^{3+}$, $Fe(CN)_6^{3-}$, and Fe^{3+}, respectively. The Fe^{3+} redox mediator has been shown to be sensitive to surface oxides. The presence of surface oxides accelerates the electron transfer [33,34]. In this case the difference of 538 mV indicates a reduced content of oxides on the RGO's surface. Hence the $Ru(NH_3)_6^{3+}$ was the best redox mediator followed very closely by $Fe(CN)_6^{3-}$, both mediators have been shown to have higher apparent heterogeneous electron transfer rate constants than Fe^{3+} redox mediator on RGO surface [35]. However the Fe^{3+} redox mediator can be used as an indicator of the presence of surface oxides.

Fig. 3. shows the electrochemical characterization of Pt and Pt/RGO electrodes by EIS in 0.5 M H_2SO_4 solutions. The Nyquist plots for Pt and Pt/RGO are shown in Fig. 3-a and Fig. 3-b, respectively. The equivalent circuit used to adjust the data is shown in the inset of each figure. The adjustment of the data to the equivalent circuits is shown as a continuous line and the experimental data are shown as dots. The equivalent circuits are composed of:

Re: electrolyte resistance between the reference and the working electrode.

CPE: constant phase element simulating the non-ideal behavior of the capacitor. It is composed of CPE-T which gives the value of pseudo-capacitance at the electrolyte/RGO interface and CPE-P which gives an idea about the behavior of the CPE. When CPE-P is equal to 1, the CPE is equal to a capacitor (C). If CPE-P equals 0.5, the CPE represents the case of semi-infinite linear diffusion (and a straight line with 45 degree slope would be recorded on the Nyquist diagram).

Rct: corresponding to the charge transfer resistance at the Pt/electrolyte interface, in parallel with the CPE element. The combination in parallel of CPE and Rct is responsible for the depression of the semicircle. This element only appears on the Pt electrode since Pt/RGO presents a capacitive behavior as observed previously by CV.

If the Nyquist plots for both samples are compared, the differences can be easily observed. The charge transfer process (Rct) is responsible for the appearance of the semicircle on Pt electrode characterization (Fig. 3-a). In the Pt/RGO sample, the capacitive behavior predominates as can be seen from the almost vertical line obtained in the Nyquist plot (Fig. 3-b). The inclination of the line indicates the deviation from the ideal capacitive behavior, represented by the CPE in the equivalent circuit. If it were a pure capacitor, a vertical line should be obtained. Table 1 shows the values of the parameters obtained after fitting data with the corresponding equivalent circuits. The most noteworthy fact is the increase in the pseudo-capacitance when Pt was coated with RGO (an increase of around 56 times was obtained). This increase of capacitance is attributed to the large surface area of RGO coating and the presence of the remaining surface oxides [36]. The value of CPE-P was in both cases close to 1, this fact indicates that the CPE behaves as a capacitor. The value of charge transfer resistance obtained for Pt was $1.77 \cdot 10^{-5}$ Ω.

3.3. Scanning electrochemical microscopy characterization

SECM was used to test the electroactivity of the Pt/RGO coatings with different redox mediators ($Fe(CN)_6^{3-}$, $Ru(NH_3)_6^{3+}$ and Fe^{3+}). SECM technique was operated under feedback mode, where the reduction tip current of the redox mediator is registered as the microelectrode approaches the surface of the sample to study. In this study, the different redox mediators were reduced on the surface of the microelectrode, then the reduction current was measured. The potential of the microelectrode was fixed at -0.1 V, 0 V and -0.4 V for Fe^{3+}, $Fe(CN)_6^{3-}$ and $Ru(NH_3)_6^{3+}$, respectively. At these potentials, the oxidized form of the redox mediator (Ox) is reduced (Red) on the microelectrode's surface at diffusion controlled rate (i_∞). The measured reduction diffusion current is defined as $i_\infty = 4 \cdot n \cdot F \cdot D \cdot C \cdot a$, where n is the number of electrons, F is the Faraday constant, D is diffusion coefficient, C is the bulk concentration of the redox mediator and a is the radius of the microelectrode tip.

In approach curves, the normalized reduction current registered at the microelectrode (I) is represented vs. the normalized distance (L). The normalized current is defined as follows: $I = i/i_\infty$ where i is the current measured at the microelectrode tip at a defined normalized distance and i_∞ is the diffusion current defined above. The normalized currents depend on RG ($RG=Rg/a$), where Rg is the radius of the insulating glass surrounding the Pt tip of radius a and the normalized distance L; where $L=d/a$ (d is the microelectrode-substrate separation). The RG of the microelectrode used in this work was $RG \geq 20$.

Depending on the conductivity of the sample, as well as the distance between the microelectrode and sample, different situations can arise:

- If the microelectrode is far enough from the surface of the sample, no interaction between the microelectrode and the sample is observed. In this case, the diffusion reduction current of the redox mediator is achieved (i_∞). By definition, the normalized current (I) is equal to 1.
- When the microelectrode approaches the surface of the sample and there is an interaction between the sample and electrode, two situations can take place depending on the conductivity of the sample:
    - If the sample is insulating, when the microelectrode approaches the surface of the sample, there is a hindrance to the diffusion of reduced redox species (Red) due to the low distance between microelectrode and sample. The surface of the sample is not able to regenerate (oxidize) (Ox) the reduced form of the redox mediator (Red). As the distance between microelectrode and sample becomes smaller, the diminution of the current is greater. In this case the normalized current (I) is lower than 1, since values of reduction current are lower than that of the diffusion current (i_∞). This case is known as negative feedback.
    - Conversely, if the sample is conductive, when the microelectrode approaches a conductive substrate, there is an increase in the reduction current of the redox mediator registered. The surface of the sample is able to regenerate (oxidize) (Ox) the reduced form of the redox mediator (Red). As the microelectrode approaches the surface of the sample the effect is increased, since a greater flux of Ox species is present. In this case, the normalized current (I) is higher than 1, since values of reduction current are higher than that of the diffusion current (i_∞). This case is known as positive feedback.

Experimental approach curves were compared with a theoretical approach one for the positive feedback model, according to equation 1. According to Rajendran el al. [37], Pade's approximation gives a close and simple equation with less relative error for all distances and is valid for RG > 10. The approximate formula of the steady-state normalized current assuming positive feedback for finite conductive substrate together with finite insulating glass thickness is:

$$I_T{}^C = \left[\frac{1 + 1.5647/L + 1.316855/L^2 + 0.4919707/L^3}{1 + 1.1234/L + 0.626395/L^2} \right] \quad (1)$$

Fig. 4 shows the SECM characterization of the Pt/RGO electrodes with the different redox mediators. First of all, the microelectrode was positioned above the Pt/RGO wire. In order to achieve a proper location of the microelectrode, the reduction current of the redox mediator was measured with the microelectrode at a constant height (z) above the sample as the microelectrode moved laterally in the x direction. The maximum current was obtained in the center of the wire since the gap between microelectrode and sample was minimal. At this position, when the microelectrode approaches the Pt/RGO surface, a positive feedback situation was observed and an increase in the reduction current was observed. The exception to this behavior was the Fe^{3+} redox mediator, where slight positive feedback or even negative feedback was obtained (Figure not shown). These results are consistent with the fast and reversible behavior of $Ru(NH_3)_6^{3+}$ and $Fe(CN)_6^{3-}$ compared to Fe^{3+} (Fig. 2).

Fig. 4-a, b, c, shows the different approach curves obtained with the different redox mediators. In the case of $Ru(NH_3)_6^{3+}$ and $Fe(CN)_6^{3-}$ redox mediators, values of positive feedback around 1.7-1.8 were obtained. For the case of Fe^{3+}, slight values of positive feedback or even negative feedback were obtained. The values of positive feedback

reported in bibliography have been around 1.7 (L=0.5) for graphene obtained by chemical vapor deposition and employing FeMeOH as mediator [15].

3.4. Dyes characterization on Pt/RGO electrodes

3.4.1. Methylene Blue characterization

Fig. 5-a shows the voltammetric characterization of a Pt/RGO electrode in $5 \cdot 10^{-3}$ M Methylene Blue / 0.5 M H_2SO_4 solution. The apparition of a redox pair with the cathodic peak at +0.23 V and the anodic one at +0.26 V can be observed. This redox pair has been attributed to the reduction of methylene blue (MB) to leucomethylene blue (LMB) [38]. Different scan rates were used to characterize the electrochemical behavior of the dye on the Pt/RGO electrode and it was observed that this process was diffusion controlled (figure not shown). The intensity of the anodic and cathodic peaks after subtracting the background current arising from RGO deposit was not proportional to the scan rate. The intensity of both peaks was proportional to the square root of the scan rate, indicating a diffusion controlled process that takes place on the RGO/electrolyte interface. The representation of log (I) vs. the scan rate also gave a slope near to 0.5 for both peaks, confirming a diffusion controlled process. Hence, this redox peak is attributed to the redox processes of dye in solution.

There was little variation of the redox pair due to the dye in solution with the number of scans. However, as the scan number increased the appearance of a new redox pair at around +0.15 V could be seen, and the intensity of this pair increased with the scan number as can be observed in Fig. 5-a. The appearance of this redox pair at lower potentials was attributed to the adsorption of the dye species [38]. After 100 scans, the Pt/RGO-MB electrode was taken out from solution and washed with ultrapure water

several times in order to remove the dye not adsorbed. Afterwards, the electrode was characterized in 0.5 M H_2SO_4 solution to evaluate the adsorbed species. Fig. 5-b shows the characterization of Pt/RGO electrode prior and after MB adsorption (electrochemical adsorption). The apparition of a redox pair with the anodic peak at +0.16 V and the cathodic one at +0.14 V could be observed. The peak to peak potential difference that was close to 0 mV, the current (I) of oxidation and reduction peaks and their electrical charge, which were almost equal, indicated that the process was adsorption controlled.

Fig. 5-c shows the voltammetric characterization of Pt/RGO-MB electrode obtained after electrochemical adsorption in 0.5 M H_2SO_4 solution using different scan rates. No significant variation of the peak potentials was observed with the scan rate, indicating a surface-confined process with fast electron transfer [23]. In Fig. 5-d, the intensity of the anodic and cathodic peaks is represented vs. the scan rate used. The RGO contribution to the intensity of both peaks was subtracted. The representation of I vs. scan rate was linear, indicating that in this case, the process was adsorption controlled. On the other hand, the representation of I vs. $\nu^{1/2}$ was not linear, excluding a diffusion controlled process (figure not shown). The representation of log(I) vs. log(ν) gave also a linear dependence with slope close to 1, confirming an adsorption controlled process.

The number of electrons involved in the process was calculated by means of the following equation [39]:

$$i_p = \frac{n \cdot F \cdot Q \cdot \nu}{4 \cdot R \cdot T} \rightarrow \frac{i_p}{\nu} = \frac{n \cdot F \cdot Q}{4 \cdot R \cdot T} \rightarrow n = \frac{slope \cdot 4 \cdot R \cdot T}{F \cdot Q} \quad (1)$$

Where:

i_p, is the intensity of the anodic or cathodic oxidation peaks (A).

n, is the number of electrons involved in the reaction.

Slope, is the slope obtained in the representation of i_p vs. ν.

ν, is the scan rate (V s^{-1}).

F, is the Faraday constant (96485 C mol^{-1}).

T, is the temperature (298 K).

Q, is the charge associated with the anodic or cathodic peak (C).

R, is the gas constant (8.31 V C K^{-1} mol^{-1}).

The number of electrons involved in the reaction was calculated by means of Eq. 1, giving a value of 1.17 and 0.92 electrons for anodic and cathodic processes, respectively. Hence the number of electrons transferred is 1 and the deviations could be due to experimental errors.

To characterize the stability of the Pt/RGO-MB electrode, it was cycled for 100 scans in 0.5 M H_2SO_4 solution. A gradual reduction of the peaks' intensity with the scan number until it stabilized. The loss of intensity could be attributed to the loss of part of the dye adsorbed on RGO's surface. Fig. 6 shows the representation of I/I_0 ratio for anodic and cathodic peaks, as can be seen there is an initial decrease and it stabilizes around a value higher than 0.6 for 100 scans.

Another experiment was performed to characterize the spontaneous adsorption of MB on the Pt/RGO electrode. For this reason, the Pt/RGO electrode was placed in contact with the dye solution, with the same electrochemical configuration previously used. However, in this case no potential was imposed. Starting from 0 V, the potential was allowed to reach its ocp and was monitored vs. time. The time used to perform the

adsorption was the same time used to perform the 100 CV scans at 50 mV s^{-1} (1 h). The potential tended toward +0.38 V after an hour of measurement (figure not shown). After this adsorption's phase, the Pt/RGO-MB electrode was washed several times with water and characterized in 0.5 M H_2SO_4 solution by CV (Fig. 5-b, blue line). The same oxidation and reduction peaks observed previously with electrochemical adsorption due to MB adsorption appeared in the voltammogram. Both peaks were also adsorption controlled since the intensity of the peak was proportional to the scan rate used. Fig. 5-b shows the comparison of the voltammograms of a Pt/RGO-RB electrode obtained electrochemically and another obtained at ocp. As can be seen, the values of current obtained with the electrochemically obtained Pt/RGO-MB electrode doubled the values obtained with the Pt/RGO-RB electrode synthesized at ocp. This indicates that the electrochemical adsorption is more efficient than the natural adsorption. The electrochemical adsorption allows the assembly of more MB molecules on the RGO structure. The charge (C) of the anodic and cathodic peaks was also approximately 3 times higher in the case of electrochemical adsorption. For example, the electrical charge for the reduction peak was 455 μC cm^{-2} for the Pt/RGO-MB electrode obtained electrochemically vs. 149 μC cm^{-2} for the Pt/RGO-MB electrode obtained at ocp.

3.4.2. Procion Orange MX-2R characterization

Fig. 7-a shows the characterization of the PMX2R adsorption on Pt/RGO electrodes by CV. The adsorption was performed in a $5 \cdot 10^{-3}$ M PMX2R / 0.5 M H_2SO_4 solution for 100 scans. The 1st, 10th, 30th, 50th and 100th voltammograms have been represented in the same figure to observe the evolution. From the 1st voltammogram, an oxidation peak appeared at +0.44 V and a reduction one appeared at +0.36 V after the 2nd scan. This

peak is attributed to the oxidation and reduction of dye in solution, respectively. As the scan number performed increased, a new oxidation peak appeared around +0.37 V (in addition to the one observed at +0.44 V), both peaks were superimposed and can be observed in the 100^{th} scan. The appearance of the new peak can be ascribed to the adsorbed dye, in the same way that happened for MB. The reduction peak at +0.36 V also increased its intensity with the number of scans, indicating the adsorption of the dye. After the 100^{th} scan, the electrode was taken out from solution and rinsed several times with ultrapure water. Thereafter, the electrode was characterized in 0.5 M H_2SO_4 to observe the adsorbed products (Fig. 7-b). The Pt/RGO voltammetric response has also been represented for comparison. As can be seen, a redox pair appeared at around +0.37 V. As in the Pt/RGO-MB electrode, the peak to peak potential difference was nearly 0 mV, the current (I) of oxidation and reduction peaks and their electrical charge was almost equal, pointing out an adsorption controlled process.

Different scan rates were used to characterize the adsorption product on the surface of the Pt/RGO electrode (5, 10, 25, 50, 100, 150, 200, 250, 300, 350, 400, 450 and 500 mV s^{-1}) (Fig. 7-c). No variations were observed in the peak potentials when varying the scan rate, indicating a surface-confined process with fast electron transfer as took place with MB. The peak intensity (I) of oxidation and reduction processes was represented vs. the scan rate used (Fig. 7-d). To calculate the intensity of oxidation and reduction peaks, the background current arising from RGO coating contribution was subtracted. As the peak intensities were proportional to the scan rate used (ν), this indicated that the process was adsorption controlled. The representation of I vs. $\nu^{1/2}$ was not linear meaning there was no diffusion controlled process (Figure not shown). The log (I) was represented vs. the log (ν) for both processes and both slopes tended to 1, confirming an adsorption

controlled process (Figure not shown). The number of electrons involved in the redox process was also 1.

The stability of the Pt/RGO-PMX2R electrode was tested by cyclic voltammetry for 100 scans in 0.5 M H_2SO_4 solution (Fig. 8). As can be seen, the intensity of oxidation and reduction peaks was progressively reduced. However, the diminution of both adsorption peaks on the Pt/RGO-PMX2R electrode was lower than in the case of the Pt/RGO-MB one. The current ratios (I/I_0) for oxidation and reduction peaks after 100 scans was 0.75 and 0.88, respectively (Fig. 8). The adsorption of PMX2R is more stable than the MB one. The adsorption of dyes on graphene substrate is dominated by π-π stacking and hydrophobic interactions [23]. The increased stability of adsorbed PMX2R could be due to the presence of chlorotriazine groups in the dye structure that could serve as fixation points with the remaining functional groups of RGO.

Another experiment was performed to observe the spontaneous adsorption of the PMX2R dye. For this reason, the Pt/RGO was placed in contact with the dye solution as it was performed for the MB ocp adsorption. The potential tended to +0.37 V (Figure not shown). After this adsorption phase, the Pt/RGO-PMX2R electrode was washed several times with water and characterized in 0.5 M H_2SO_4 solution (Fig. 7-b). The same oxidation and reduction peaks were obtained; however, in this case, the intensity of the dye's peaks in relation to the RGO voltammetric background was lower. The process was also adsorption controlled since the peak intensity was proportional to the scan rate and not to the square root of the scan rate (Figure not shown). Fig. 7-b compares the voltammograms after OCP and electrochemical adsorption. As can be seen, the voltammetric adsorption produce an increase in the anodic and cathodic current peaks when compared with OCP adsorption. The electrochemical adsorption is more efficient in the adsorption of PMX2R. The charge (C) of the anodic and cathodic

peaks was also approximately 6 times higher in the case of electrochemical adsorption. For example, the electrical charge for the reduction peak was 162 μC cm^{-2} for the Pt/RGO-PMX2R electrode obtained electrochemically vs. 26 μC cm^{-2} for the Pt/RGO-PMX2R electrode obtained at ocp.

3.4.3. Amaranth characterization

Fig. 9-a shows the voltammetric characterization of a Pt/RGO electrode in $5 \cdot 10^{-3}$ M Amaranth / 0.5 M H_2SO_4 solution. In the first scan, two peaks appeared, one anodic peak at +0.44 V and one cathodic peak at -0.05 V. The anodic peak suffered a reduction in intensity with the increasing number of scans, however the potential at which this took place was not displaced. On the other hand, the cathodic peak suffered a reduction in intensity and the potential at which the process took place was also displaced towards lower potentials. After the 100 adsorption scans, the electrode was washed several times with ultrapure water and characterized in 0.5 M H_2SO_4. Fig. 9-b shows the comparison of the voltammograms before and after amaranth adsorption. After dye adsorption some redox processes appear between 0 and +0.4 V. However they are not as defined as they were in the case of MB or PMX2R.

The usefulness of CV to monitor the adsorption of dyes on Pt/RGO electrodes was demonstrated. The quantity of dye adsorbed is substantially increased when compared with ocp adsorption. Reduced graphene oxide (RGO) structure presents zones were the sp^2 structure of pristine graphene has been restored but also presents other zones were functional groups are still present [21]. The main mechanisms of adsorption of the dyes on RGO are π–π stacking and hydrophobic interactions on the zones where the sp^2 structure has been restored and charge transfer on the zones where the functional groups

are still present. Hence, the mechanism of adsorption will depend on the structure of the dye [24]. Graphene oxide (GO) has been shown to be a good adsorbent for cationic dyes due to its negatively charged surface which increase electrostatic interaction between the cationic dye and GO [24]. For the same reason GO is not good for the adsorption of anionic dyes since both of them present negative charges and electrostatic repulsion takes place. Reduced graphene oxide (RGO) presents affinity for both of them, being higher in the case of anionic dyes (95% for anionic dyes and 50% for cationic dyes) [24]. The electrochemically-induced adsorption enhances the adsorption of the dye due to the polarization of the RGO surface and the creation of electrostatic interaction between the dye and the RGO surface. Small influence should be expected for dyes with low polarity. The CV induced adsorption could also be used to increase the adsorption of other products, which adsorption on graphene derivatives has been reported. For instance, the enzyme adsorption for the production of biosensors [25,40-44] or enzymatic biofuel cells [44]. This procedure would increase the sensibility of the biosensors.

4. Conclusions

Reduced graphene oxide (RGO) coated Pt electrodes were obtained by electrochemical reduction. The Pt/RGO electrodes were characterized by cyclic voltammetry (CV) and electrochemical impedance spectroscopy (EIS), showing the appearance of the capacitive behaviour of RGO. The electrochemically obtained RGO coated electrodes were characterized by scanning electrochemical microscopy (SECM) for the first time. The coatings obtained were homogeneous and with good electroactivity. The influence

of the redox mediator used in the response obtained was clearly shown. The peak to peak potential separation obtained from the voltammograms of the different redox mediators on Pt/RGO electrodes was 101, 121 and 538 mV for $Ru(NH_3)_6^{3+}$, $Fe(CN)_6^{3-}$, and Fe^{3+}, respectively. With the first two redox mediators, the electronic transfer was reversible and with the Fe^{3+} one it was quite irreversible. The Fe^{3+} redox mediator is oxide sensitive and the high peak to peak potential separation indicates a low quantity of oxidized groups on the surface of RGO (indicates an effective reduction of GO) as EDX has also shown. The approach curves obtained by SECM confirmed this tendency, showing similar values of positive feedback for $Ru(NH_3)_6^{3+}$ and $Fe(CN)_6^{3-}$, and low values of positive feedback or even negative feedback for the Fe^{3+} redox mediator.

The electrochemical adsorption of different dyes (Methylene Blue (MB), Procion Orange MX-2R (PMX2R) and Amaranth (AM)) was accomplished by CV on Pt/RGO electrodes. It has been shown that this technique could be used as a technique to monitor the adsorption of the dyes. After MB and PMX2R adsorption, the voltammetric characterization in 0.5 M H_2SO_4 solution showed the appearance of a redox pair at +0.15 V and +0.36 V, respectively. The processes were adsorption-controlled. The electrochemical adsorption is more efficient than ocp adsorption which opens the possibility of employing this technique to enhance the adsorption of other substances such as enzymes for the production of biosensors.

Acknowledgements

Authors wish to thank to the Spanish Ministerio de Ciencia e Innovación (contracts CTM2011-23583 and CTM2014-52990-R) for the financial support. J. Molina is grateful to the Conselleria d'Educació, Formació i Ocupació (Generalitat Valenciana)

for the Programa VALi+D Postdoctoral Fellowship. A.I. del Río is grateful to the Spanish Ministerio de Ciencia y Tecnología for her FPI fellowship. C. García is grateful to the Conselleria d'Educació, Formació i Ocupació (Generalitat Valenciana) for her Gerónimo Forteza fellowship. Electron Microscopy Service of the UPV (Universitat Politècnica de València) is gratefully acknowledged for help with SEM and EDX characterization. Tim Vickers is gratefully acknowledged for help with English revision.

Role of the funding source

The funding sources had no involvement in the study design; in the collection, analysis and interpretation of data; in the writing of the report; and in the decision to submit the article for publication.

References

[1] K. S. Novoselov, A.K. Geim, S.V. Morozov, D. Jiang, Y. Zhang, S.V. Dubonos, I. V. Grigorieva, A. A. Firsov, Electric field effect in atomically thin carbon films, Science 306 (2004) 666.

[2] F. Schwierz, Graphene transistors, Nat. Nanotechnol. 5 (2010) 487.

[3] A.A. Balandin, Thermal properties of graphene and nanostructured carbon materials, Nat. Mater. 10 (2011) 569.

[4] F. Bonaccorso, Z. Sun, T. Hasan, A. C. Ferrari, Graphene photonics and optoelectronics, Nat. Photonics 4 (2010) 611.

[5] S. Stankovich, D.A. Dikin, G.H.B. Dommett, K.M. Kohlhaas, E.J. Zimney, E.A. Stach, R.D. Piner, S.T. Nguyen, R.S. Ruoff, Graphene-based composite materials, Nature 442 (2006) 282.

[6] R. Verdejo, M.M. Bernal, L.J. Romasanta, M.A. Lopez-Manchado, Graphene filled polymer nanocomposites, J. Mater. Chem. 21 (2011) 3301.

[7] B.Y. Zhu, S. Murali, W. Cai, X. Li , J.W. Suk, J.R. Potts, R.S. Ruoff, Graphene and graphene oxide: synthesis, properties, and applications, Adv. Mater. 22 (2010) 3906.

[8] F. Bonaccorso, A. Lombardo, T. Hasan, Z. Sun, L. Colombo, A.C. Ferrari, Production and processing of graphene and 2d crystals, Mater. Today 15 (2012) 564.

[9] S. Park, R.S. Ruoff, Chemical methods for the production of graphenes, Nat. Nanotechnol. 4 (2009) 217.

[10] S. Pei, H.-M. Cheng, The reduction of graphene oxide, Carbon 50 (2012) 3210.

[11] M. Yaldagard, N. Seghatoleslami, M. Jahanshahi, Preparation of Pt-Co nanoparticles by galvanostatic pulse electrochemical codeposition on in situ electrochemical reduced graphene nanoplates based carbon paper electrode for oxygen reduction reaction in proton exchange membrane fuel cell, Appl. Surf. Sci. 315 (2014) 222.

[12] Q. Xiang, J. Yu, M. Jaroniec, Graphene-based semiconductor photocatalysts, Chem. Soc. Rev. 41 (2012) 782.

[13] S. Bergner, P. Vatsyayan, F.-M. Matysik, Recent advances in high resolution scanning electrochemical microscopy of living cells – A review, Anal. Chim. Acta 775 (2013) 1.

[14] R.M. Souto, Y. González-García, S. González, G.T. Burstein, Damage to paint coatings caused by electrolyte immersion as observed in situ by scanning electrochemical microscopy, Corros. Sci. 46 (2004) 2621.

[15] C. Tan, J. Rodríguez-López, J.J. Parks, N.L. Ritzert, D.C. Ralph, H.D. Abruña, Reactivity of monolayer chemical vapor deposited graphene imperfections studied using scanning electrochemical microscopy, ACS Nano 6 (2012) 3070.

[16] A.G. Güell, N. Ebejer, M.E. Snowden, J.V. Macpherson, P.R. Unwin, Structural correlations in heterogeneous electron transfer at monolayer and multilayer graphene electrodes, J. Am. Chem. Soc. 134 (2012) 7258.

[17] S. Rapino, E. Treossi, V. Palermo, M. Marcaccio, F. Paolucci, F. Zerbetto, Playing peekaboo with graphene oxide: a scanning electrochemical microscopy investigation, Chem. Commun. 50 (2014) 13117.

[18] J. Azevedo, C. Bourdillon, V. Derycke, S. Campidelli, C. Lefrou, R. Cornut, Contactless surface conductivity mapping of graphene oxide thin films deposited on glass with scanning electrochemical microscopy, Anal. Chem. 85 (2013) 1812.

[19] N. Ebejer, A.G. Güell, S.C.S. Lai, K. McKelvey, M.E. Snowden, P.R. Unwin, Scanning electrochemical cell microscopy: A versatile technique for nanoscale electrochemistry and functional imaging, Annu. Rev. Anal. Chem. 6 (2013) 329.

[20] J. Molina, J. Fernández, J.C. Inés, A.I. del Río, J. Bonastre, F. Cases, Electrochemical characterization of reduced graphene oxide-coated polyester fabrics, Electrochim. Acta 93 (2013) 44.

[21] J. Molina, J. Fernández, A.I. del Río, J. Bonastre, F. Cases, Chemical and electrochemical study of fabrics coated with reduced graphene oxide, Appl. Surf. Sci. 279 (2013) 46.

[22] X. Dong, D. Fu, W. Fang, Y. Shi, P. Chen, L.-J. Li, Doping single-layer graphene with aromatic molecules, Small 5 (2009) 1422.

[23] D. Zhang, L. Fu, L. Liao, B. Dai, R. Zou, C. Zhang, Electrochemically functional graphene nanostructure and layer-by-layer nanocomposite incorporating adsorption of electroactive methylene blue, Electrochim. Acta 75 (20912) 71.

[24] G.K. Ramesha, A.V. Kumara, H.B. Muralidhara, S. Sampath, Graphene and graphene oxide as effective adsorbents toward anionic and cationic dyes, J. Colloid Interface Sci. 361 (2011) 270.

[25] M. Pumera, Graphene in biosensing, Mater. Today 14 (2011) 308.

[26] J. Balapanuru, J.-X. Yang, S. Xiao, Q. Bao, M. Jahan, L. Polavarapu, J. Wei, Q.-H. Xu, K.P. Loh, A graphene oxide–organic dye ionic complex with DNA-sensing and optical-limiting properties, Angew. Chem. Int. Ed. 49 (2010) 6549.

[27] J. Malig, N. Jux, D. Kiessling, J.-J. Cid, P. Vázquez, T. Torres, D.M. Guldi, Towards tunable graphene/phthalocyanine–PPV hybrid systems, Angew. Chem. Int. Ed. 50 (2011) 3561.

[28] N.V. Kozhemyakina, J.M. Englert, G. Yang , E. Spiecker, C.D. Schmidt, F. Hauke, A. Hirsch, Non-covalent chemistry of graphene: Electronic communication with dendronized perylene bisimides, Adv. Mater. 22 (2010) 5483.

[29] J. Clavilier, The role of anion on the electrochemical behavior of a {111} platinum surface; an unusual splitting of the voltammogram in the hydrogen region, J. Electroanal. Chem. 107 (1979) 211.

[30] L. Chen, Y. Tang, K. Wang, C. Liu, S. Luo, Direct electrodeposition of reduced graphene oxide on glassy carbon electrode and its electrochemical application, Electrochem. Commun. 13 (2011) 133.

[31] W. Si, X. Wu, J. Zhou, F. Guo, S. Zhuo, H. Cui, W. Xing, Reduced graphene oxide aerogel with high-rate supercapacitive performance in aqueous electrolytes, Nanoscale Res. Lett. 8 (2013) 247.

[32] J. Molina, J. Fernández, A.I. del Río, J. Bonastre, F. Cases, Synthesis of Pt nanoparticles on electrochemically reduced graphene oxide by potentiostatic and alternate current methods, Mat. Charact. 89 (20914) 56.

[33] R.L. McCreery, Advanced carbon electrode materials for molecular electrochemistry, Chem. Rev. 108 (2008) 2646.

[34] A. Ueda, D. Kato, N. Sekioka, S. Hirono, O. Niwa, Local imaging of an electrochemical active/inactive region on a conductive carbon surface by using scanning electrochemical microscopy, Anal. Sci. 25 (2009) 645.

[35] B.L. Tang, Y. Wang, Y. Li, H. Feng, J. Lu, J. Li, Preparation, structure, and electrochemical properties of reduced graphene sheet films, Adv. Funct. Mater. 19 (2009) 2782.

[36] W. Zhang, Y. Zhang, Y. Tian, Z. Yang, Q. Xiao, X. Guo, L. Jing, Y. Zhao, Y. Yan, J. Feng, K. Sun, Insight into the capacitive properties of reduced graphene oxide, ACS Appl. Mater. Interfaces 6 (2014) 2248.

[37] L. Rajendran, S.P. Ananthi, Analysis of positive feedback currents at the scanning electrochemical microscope, J. Electroanal. Chem. 561 (2004) 113.

[38] R. Zhan, S. Song, Y. Liu, S. Dong, Mechanisms of methylene blue electrode processes studied by in situ electron paramagnetic resonance and ultraviolet-visible spectroelectrochemistry, J. Chem. Soc. Faraday Trans. 86 (1990) 3125.

[39] P.M. Ndangili, A.N. Jijana, R.A. Olowu, S.N. Mailu, F.R. Ngece, A. Williams, T.T. Waryo, P.G.L. Baker, E.I. Iwuoha, Impedimetric response of a label-free genosensor prepared on a 3-mercaptopropionic acid capped gallium selenide nanocrystal modified gold electrode, Int. J. Electrochem. Sci. 6 (2011) 1438.

[40] M. Pumera, A. Ambrosi, A. Bonanni, E.L.K. Chng, H.L. Poh, Graphene for electrochemical sensing and biosensing, Trends Anal. Chem. 29 (2010) 954.

[41] Y. Shao, J. Wang, H. Wu, J. Liu, I.A. Aksay, Y. Lina, Graphene based electrochemical sensors and biosensors: A review, Electroanal. 22 (2010) 1027.

[42] J. Filip, J. Tkac, Effective bioelectrocatalysis of bilirubin oxidase on electrochemically reduced graphene oxide, Electrochem. Commun. 49 (2014) 70.

[43] B. Liang, X. Guo, L. Fang, Y. Hu, G. Yang, Q. Zhu, J. Wei, X. Ye, Study of direct electron transfer and enzyme activity of glucose oxidase on graphene surface, Electrochem. Commun. 50 (2015) 1.

[44] H.d. Toit, M.D. Lorenzo, Glucose oxidase directly immobilized onto highly porous gold electrodes for sensing and fuel cell applications, Electrochim. Acta 138 (2014) 86.

Figure captions

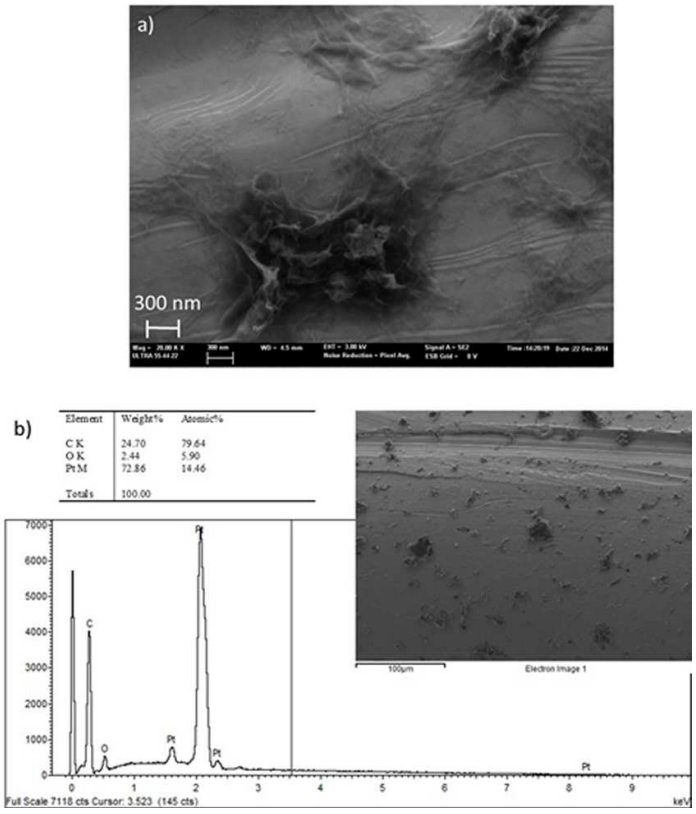

Fig. 1. a) FESEM micrograph of Pt/RGO electrode (x20000). b) EDX and FESEM micrograph of Pt/RGO electrode.

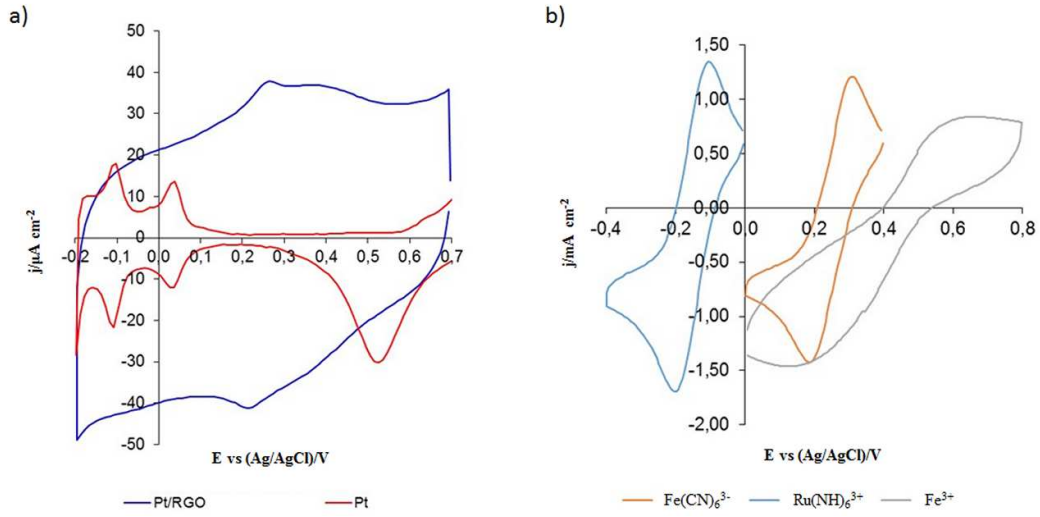

Fig. 2. a) Cyclic voltammograms of Pt and Pt/RGO electrode in 0.5 M H_2SO_4, scan rate 50 mV s^{-1}. b) Cyclic voltammograms of Pt/RGO electrode in 0.01 M $Ru(NH_3)_6^{3+}$ / 0.1 KCl, 0.01 M $Fe(CN)_6^{3-}$ / 0.1 M KCl and 0.02 M Fe^{3+} / 0.5 M H_2SO_4, scan rate 50 mV s^{-1}.

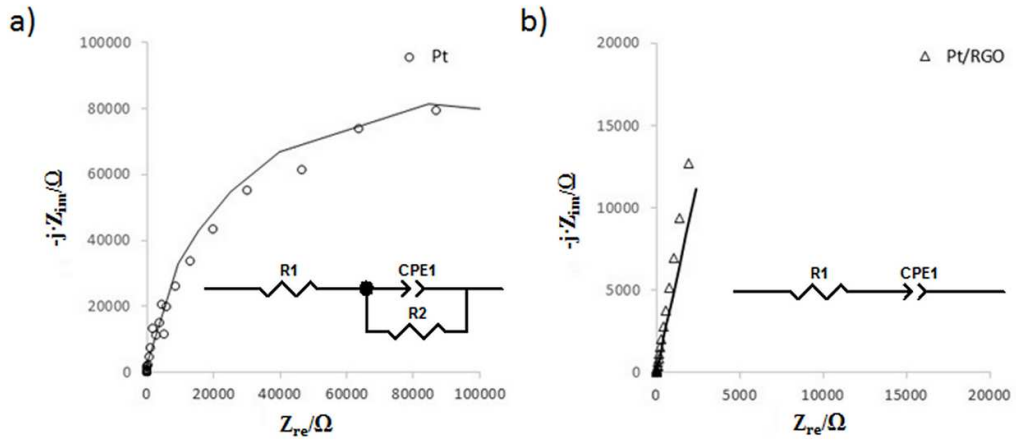

Fig. 3. Nyquist plots for EIS characterization of Pt (a) and Pt/RGO (b) electrodes in 0.5 M H_2SO_4, frequency range from 10^5 to 10^{-2} Hz.

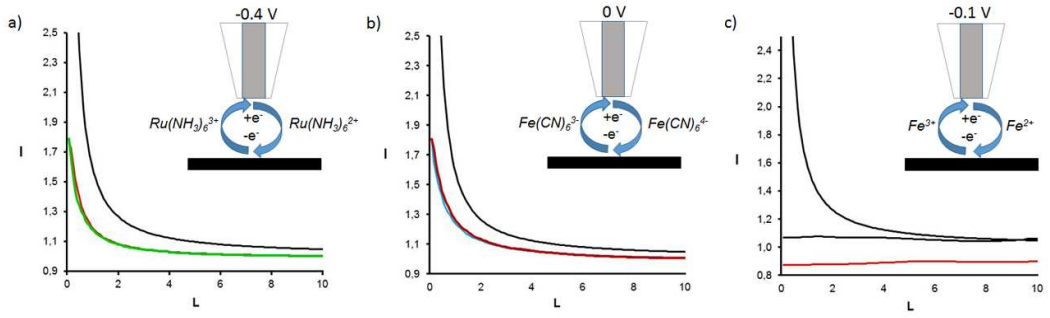

Fig. 4. 2D SECM representations for Pt/RGO wires obtained by vertical displacement of the microelectrode for the different redox systems 0.01 M $Ru(NH_3)_6^{3+}$ / 0.1 KCl (a), 0.01 M $Fe(CN)_6^{3-}$ / 0.1 M KCl (b) and 0.02 M Fe^{3+} / 0.5 M H_2SO_4 (c). Theoretical positive feedback model has been included as a black continuous line. Data obtained with a 25 μm diameter Pt tip, approach rate 10 μm s^{-1}.

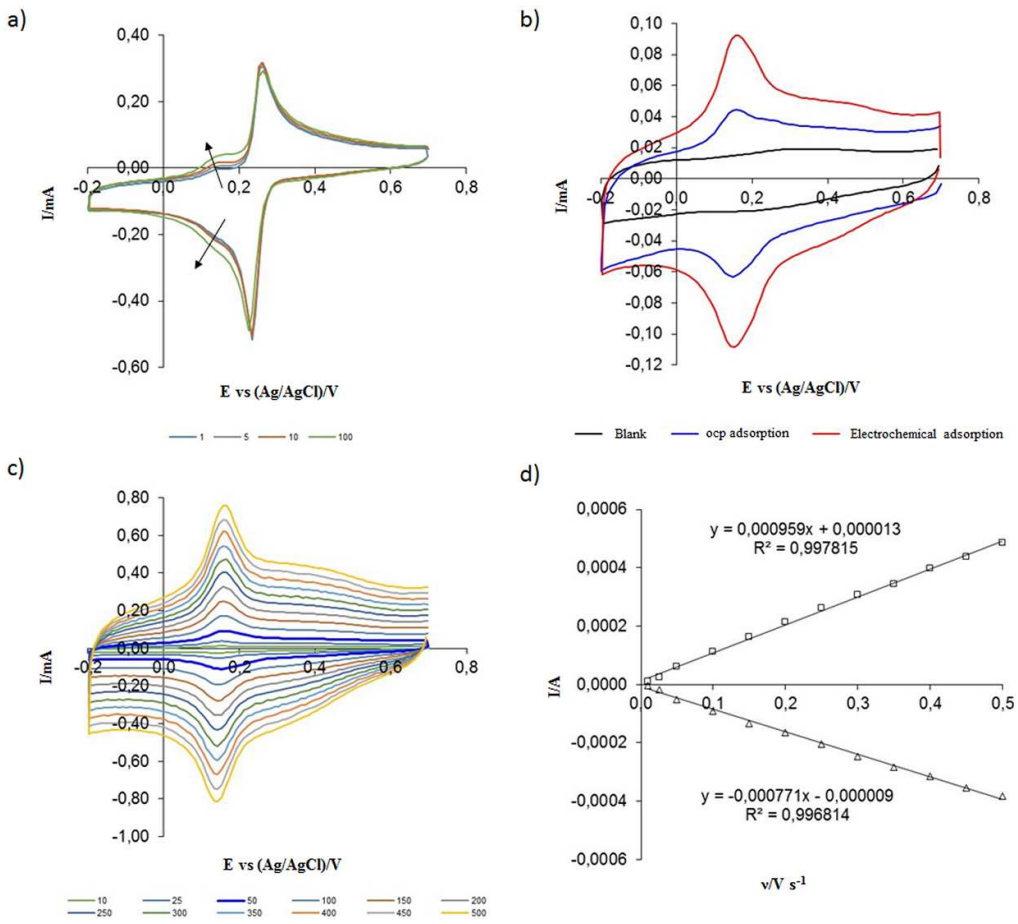

Fig. 5. a) Methylene Blue (MB) adsorption by CV on Pt/RGO electrode performed in $5 \cdot 10^{-3}$ M MB / 0.5 M H_2SO_4 solution during 100 scans (1^{st}, 5^{th}, 10^{th} and 100^{th} scans are represented). b) CV characterization of Pt/RGO electrode in 0.5 M H_2SO_4 prior and after dye adsorption performed electrochemically and at ocp. Characterization and adsorption were performed with a scan rate of 50 mV s^{-1}. c) CV characterization of Pt/RGO-MB electrode (electrochemical adsorption) in 0.5 M H_2SO_4 solution with different scan rates: 10, 25, 50, 100, 150, 200, 250, 300, 350, 400, 450 and 500 mV s^{-1}). d) Intensity (I) vs. scan rate (ν) plot.

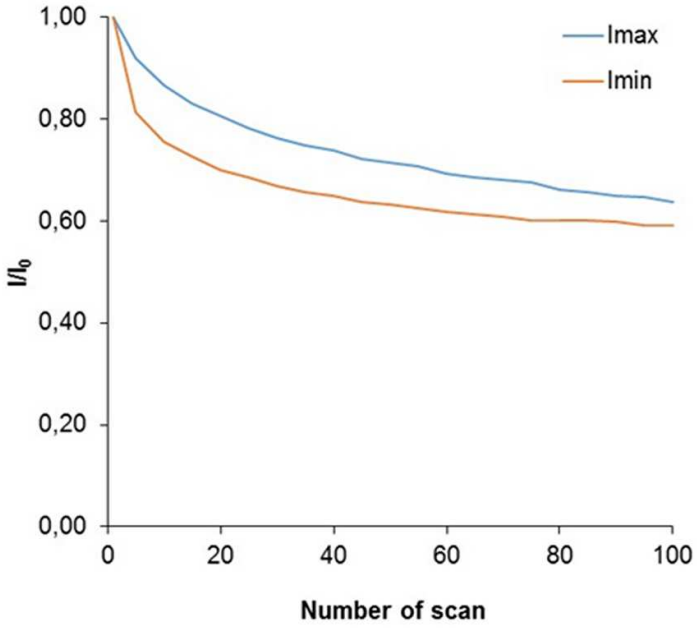

Fig. 6. I/I_0 for anodic and cathodic peaks vs. the number of scan for Pt/RGO-MB electrode in 0.5 M H_2SO_4 solution during 100 scans.

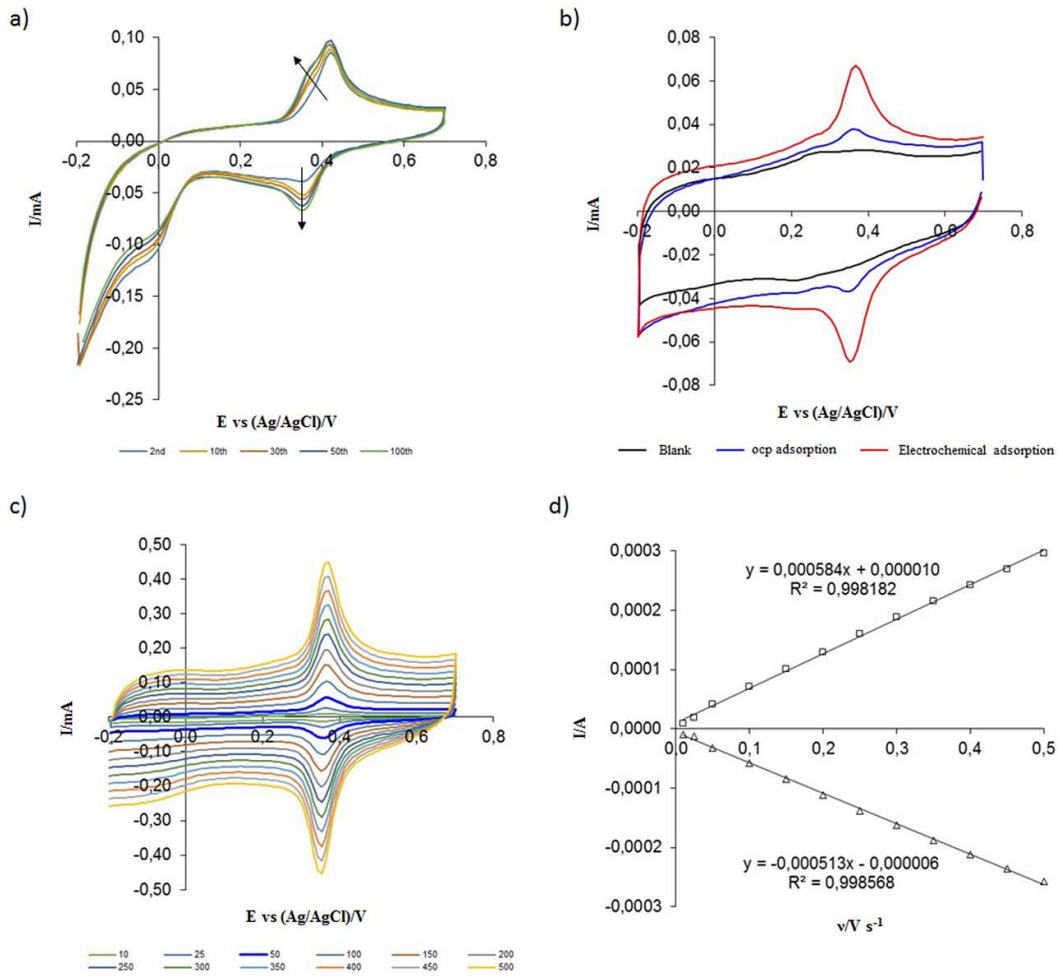

Fig. 7. a) Procion MX-2R (PMX2R) adsorption by CV on Pt/RGO electrode performed in $5 \cdot 10^{-3}$ M PMX2R / 0.5 M H_2SO_4 solution during 100 scans (2^{nd}, 10^{th}, 30^{th}, 50^{th} and 100^{th} scans are represented). b) CV characterization of Pt/RGO electrode in 0.5 M H_2SO_4 prior and after dye adsorption performed electrochemically and at ocp. Characterization and adsorption were performed with a scan rate of 50 mV s^{-1}. c) CV characterization of Pt/RGO-PMX2R electrode (electrochemical adsorption) in 0.5 M H_2SO_4 solution with different scan rates: 10, 25, 50, 100, 150, 200, 250, 300, 350, 400, 450 and 500 mV s^{-1}). d) Intensity (I) vs. scan rate (ν) plot.

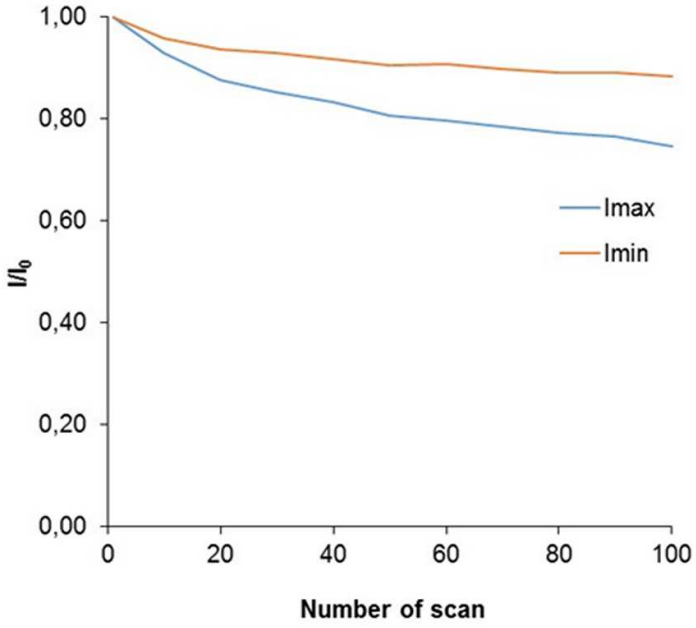

Fig. 8. I/I_0 for anodic and cathodic peaks vs. the number of scan for Pt/RGO-PMX2R electrode in 0.5 M H_2SO_4 solution during 100 scans.

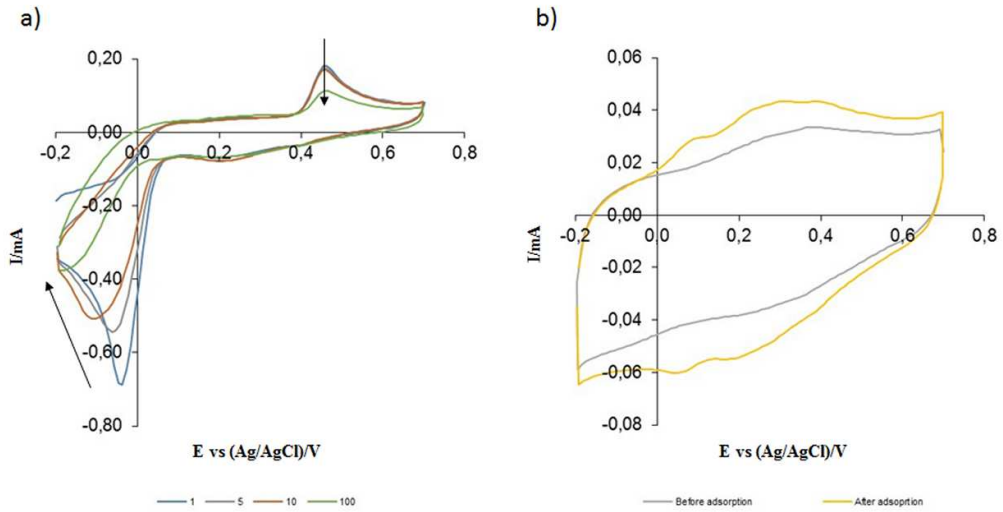

Fig. 9. a) Cyclic voltammograms of characterization of Amaranth adsorption on Pt/RGO electrode in $5 \cdot 10^{-3}$ M Amaranth / 0.5 M H_2SO_4 solution during 100 scans (1^{st},

5^{th}, 10^{th} and 100^{th} scans are represented). b) Cyclic voltammograms of Pt/RGO electrode prior and after dye adsorption. Scan rate used, 50 mV s^{-1}.

Table captions

Table 1. Results of the fitting of impedance data of Pt and Pt/RGO electrodes in 0.5 M H_2SO_4. Data adjusted with the equivalent circuits shown in Fig. 3.

Electrode	Chi-Sqr	Rs (Ω)	CPE-T ($F^{CPE-P}.\Omega^{(1-CPE-P)}$)	CPE-P	Rct (Ω)
Pt	0,09	1,59	$1{,}72\cdot10^{-5}$	0,95	$1{,}77\cdot10^{5}$
Pt/RGO	0,02	2,03	$9{,}67\cdot10^{-4}$	0,87	-

Figure(1)

Click here to download high resolution image

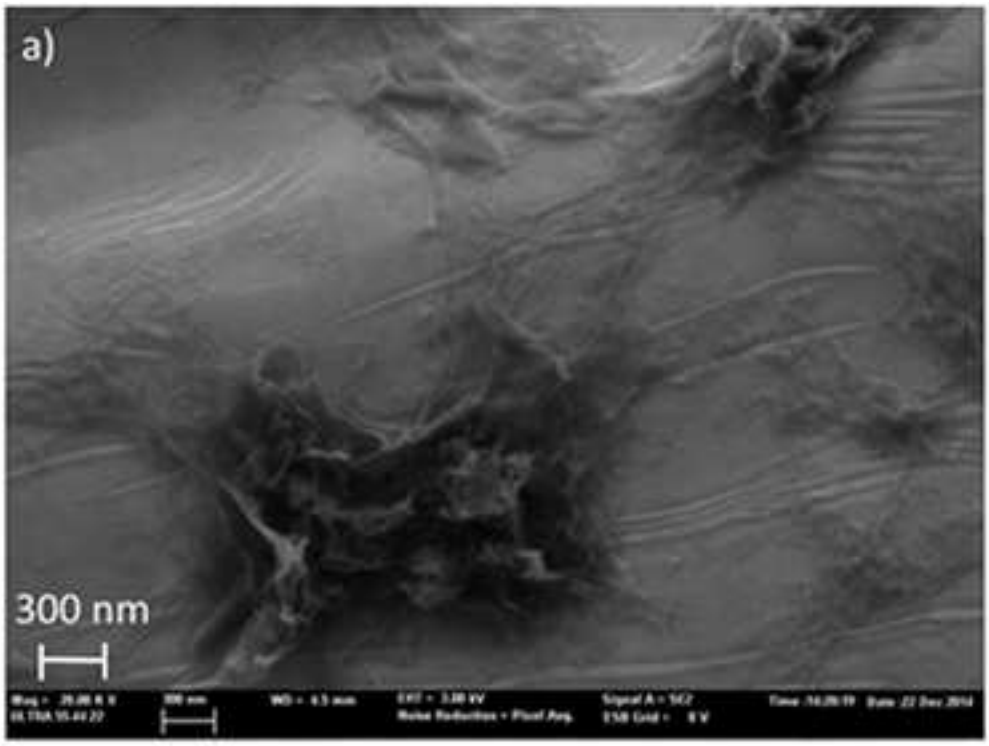

b)

Element	Weight%	Atomic%
C K	24.70	79.64
O K	2.44	5.90
Pt M	72.86	14.46
Totals	100.00	

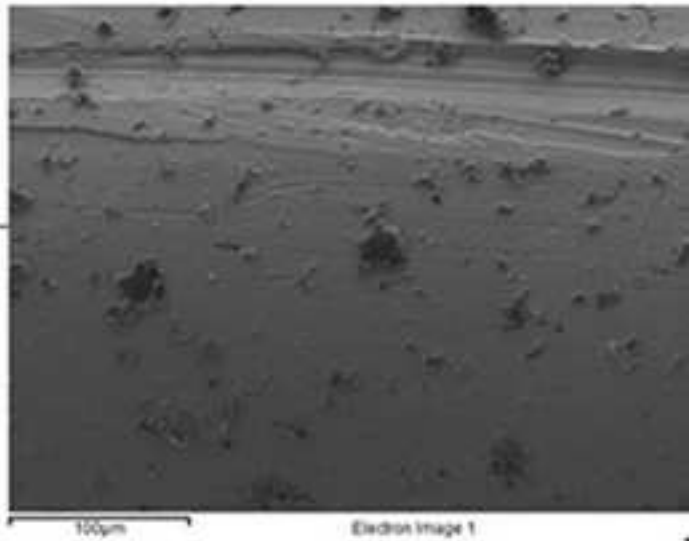

Figure(2)
Click here to download high resolution image

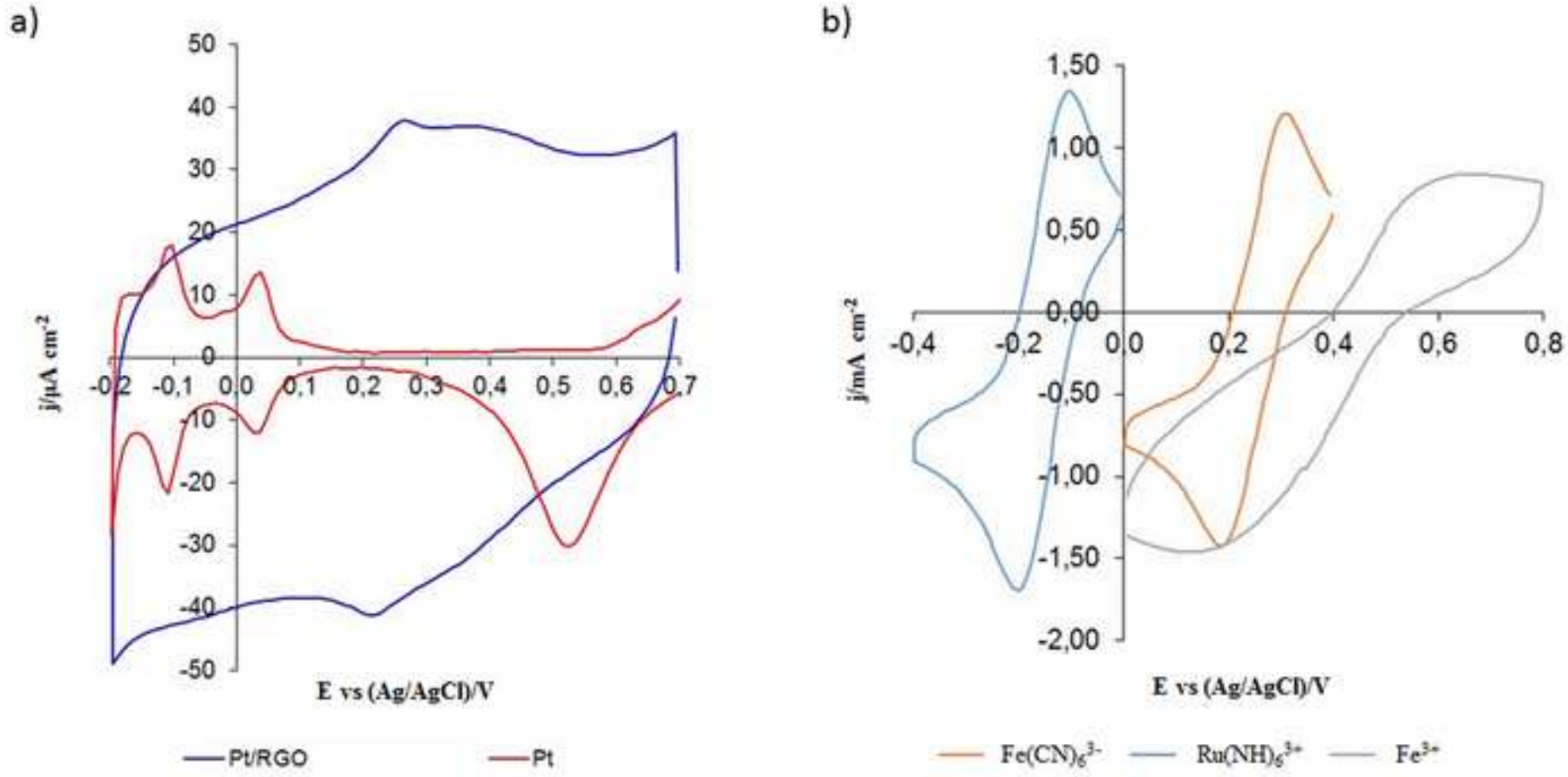

Figure(3)
Click here to download high resolution image

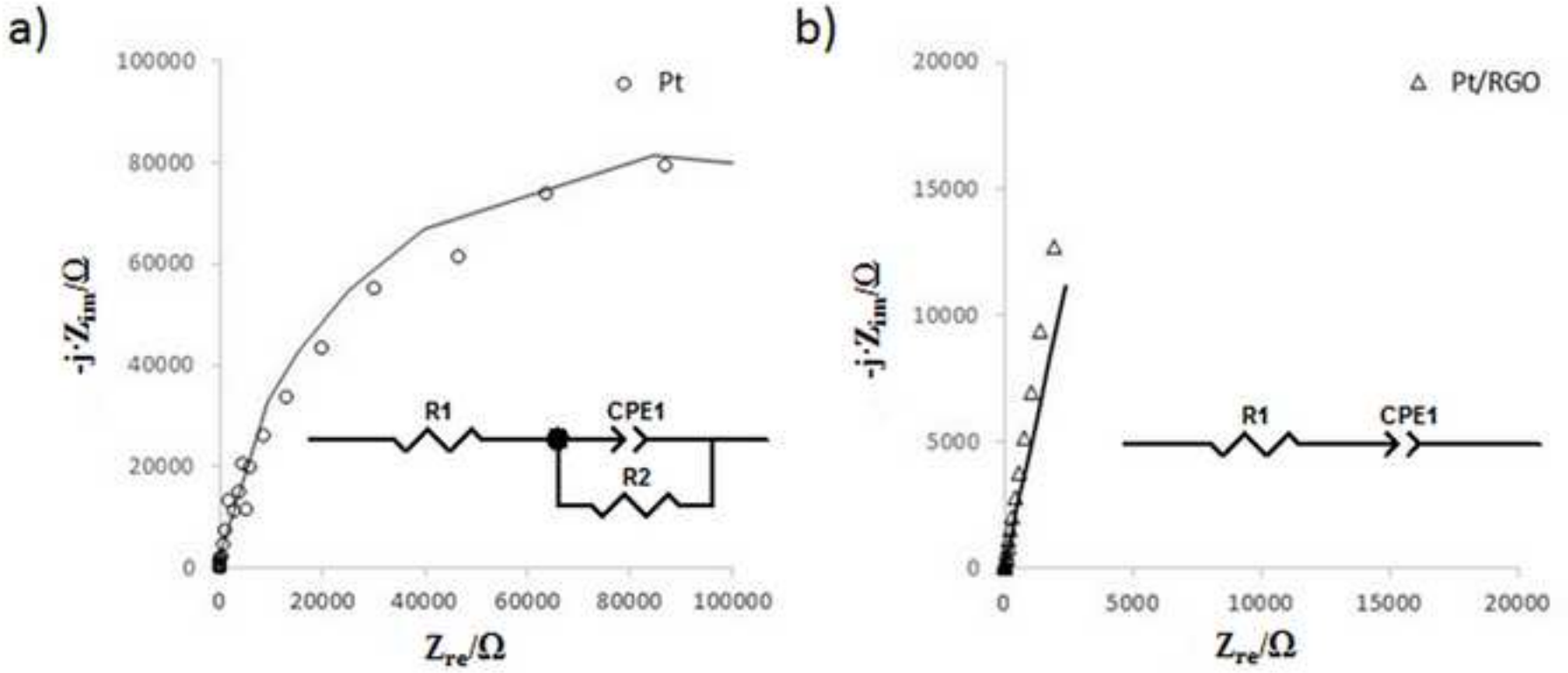

Figure(4)

Click here to download high resolution image

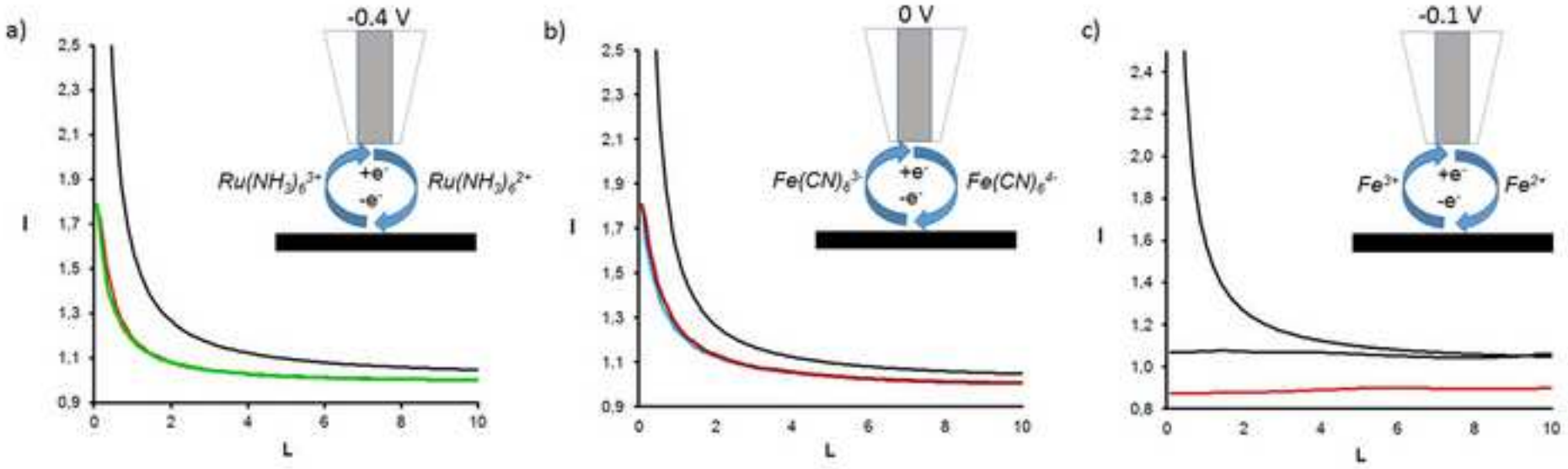

Figure(5)

Click here to download high resolution image

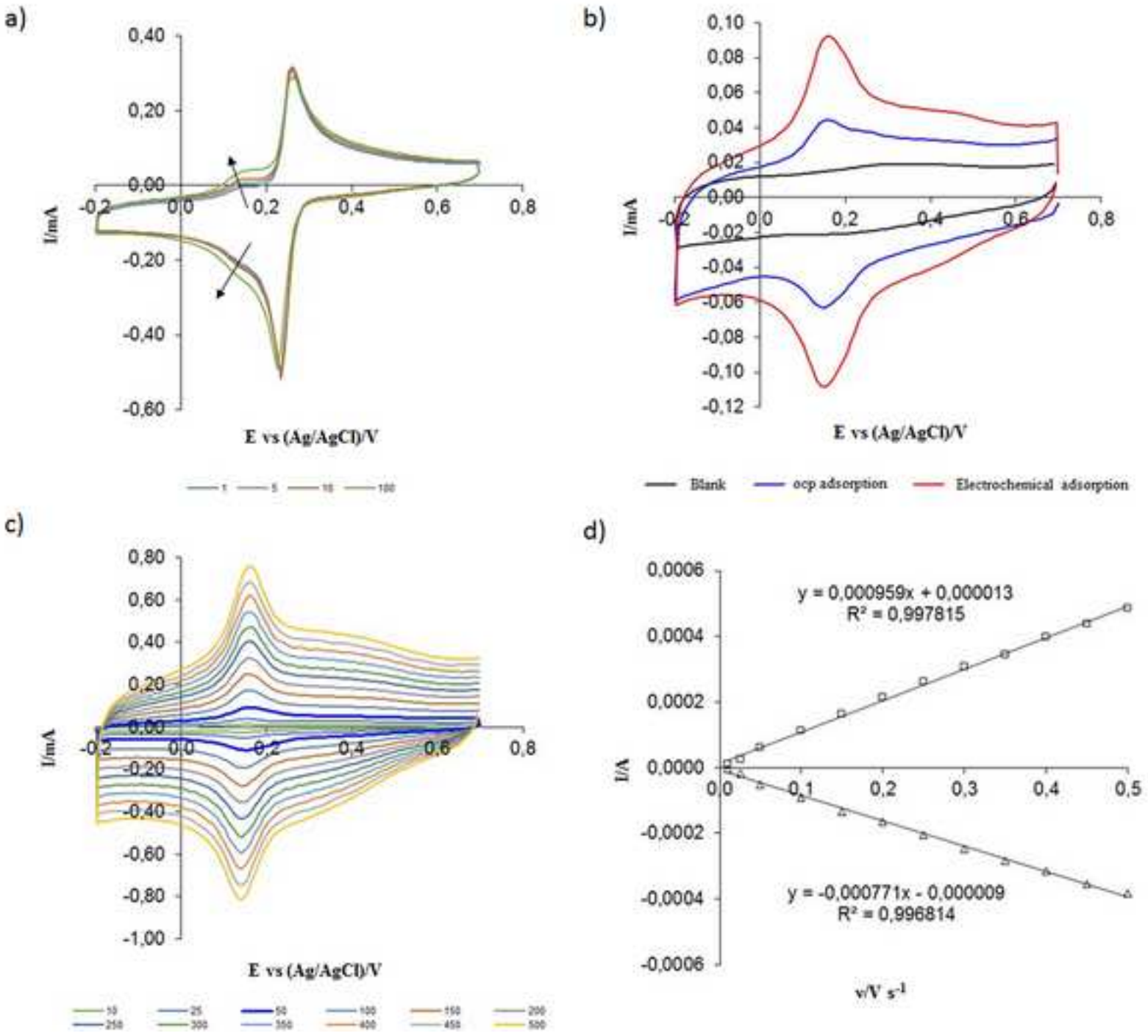

Figure(6)
Click here to download high resolution image

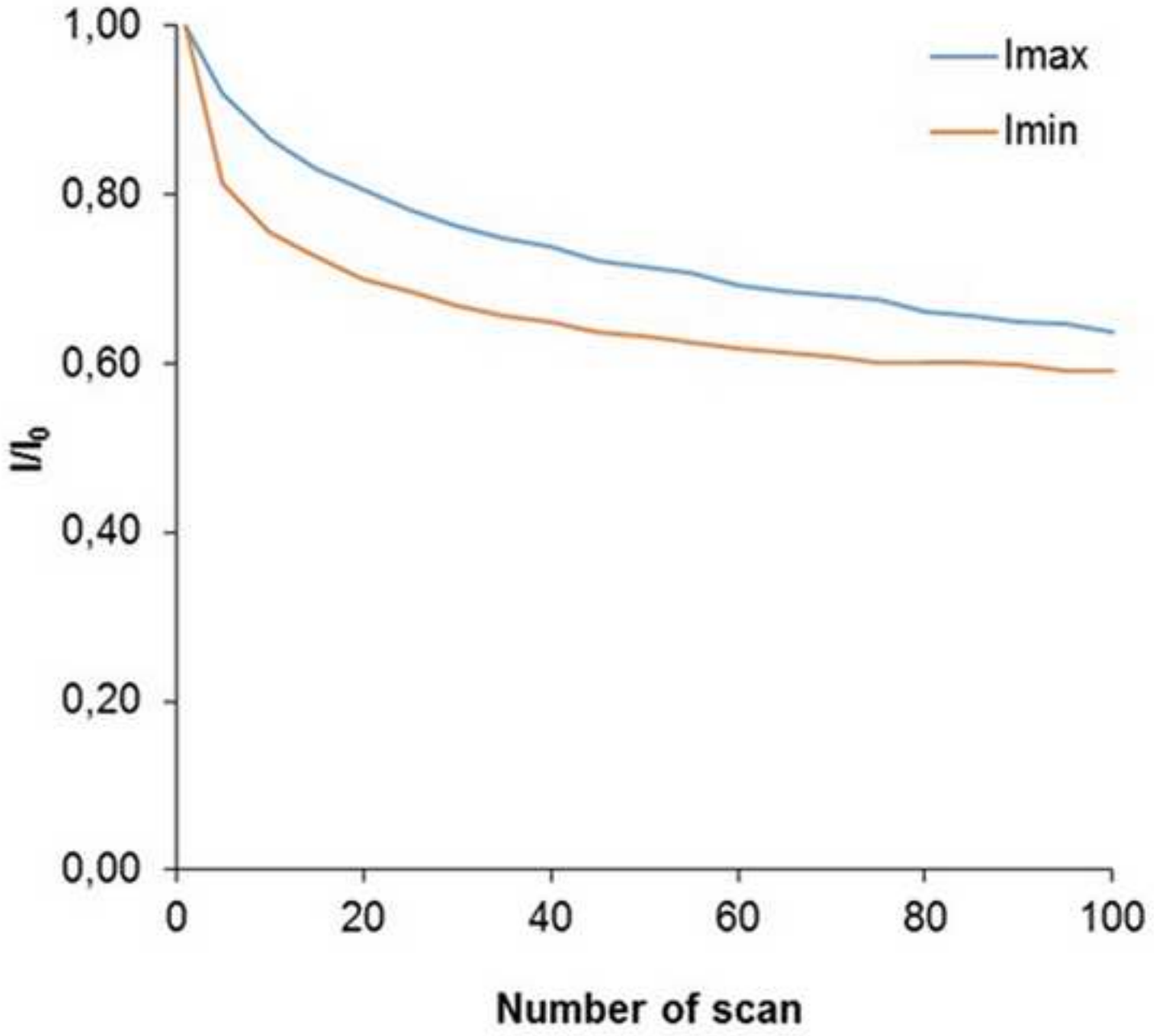

Figure(7)
Click here to download high resolution image

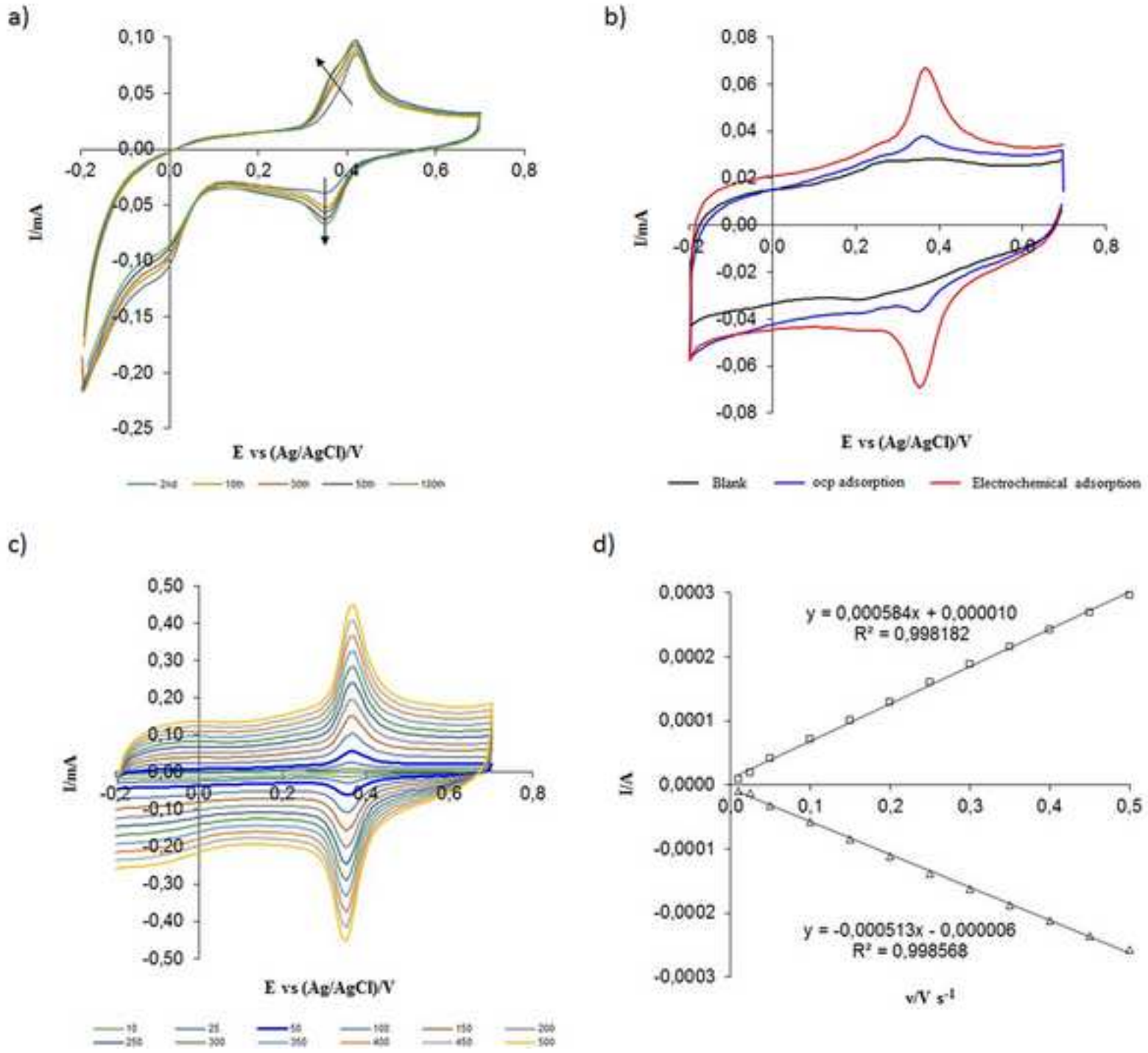

Figure(8)
Click here to download high resolution image

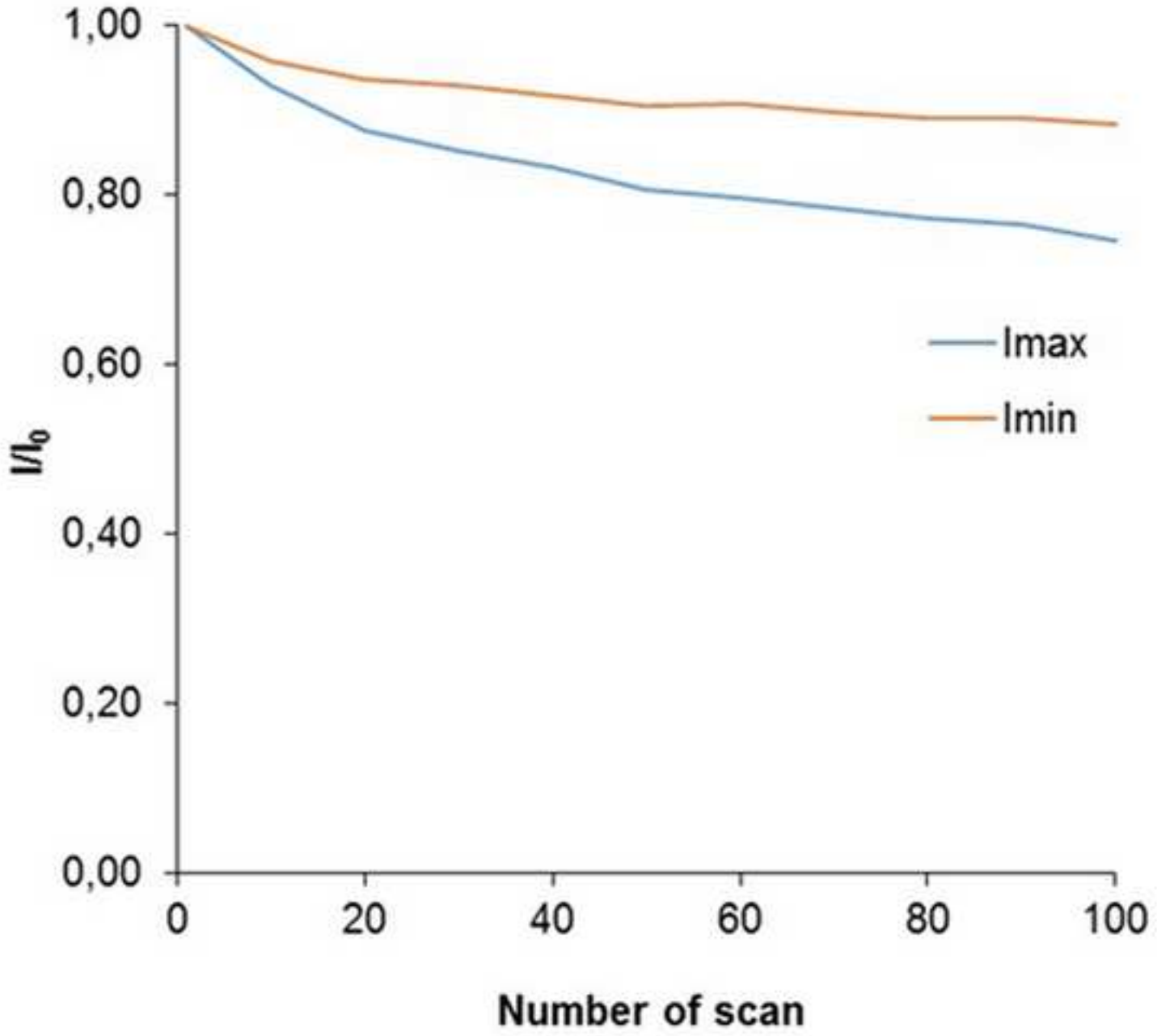

Figure(9)
Click here to download high resolution image

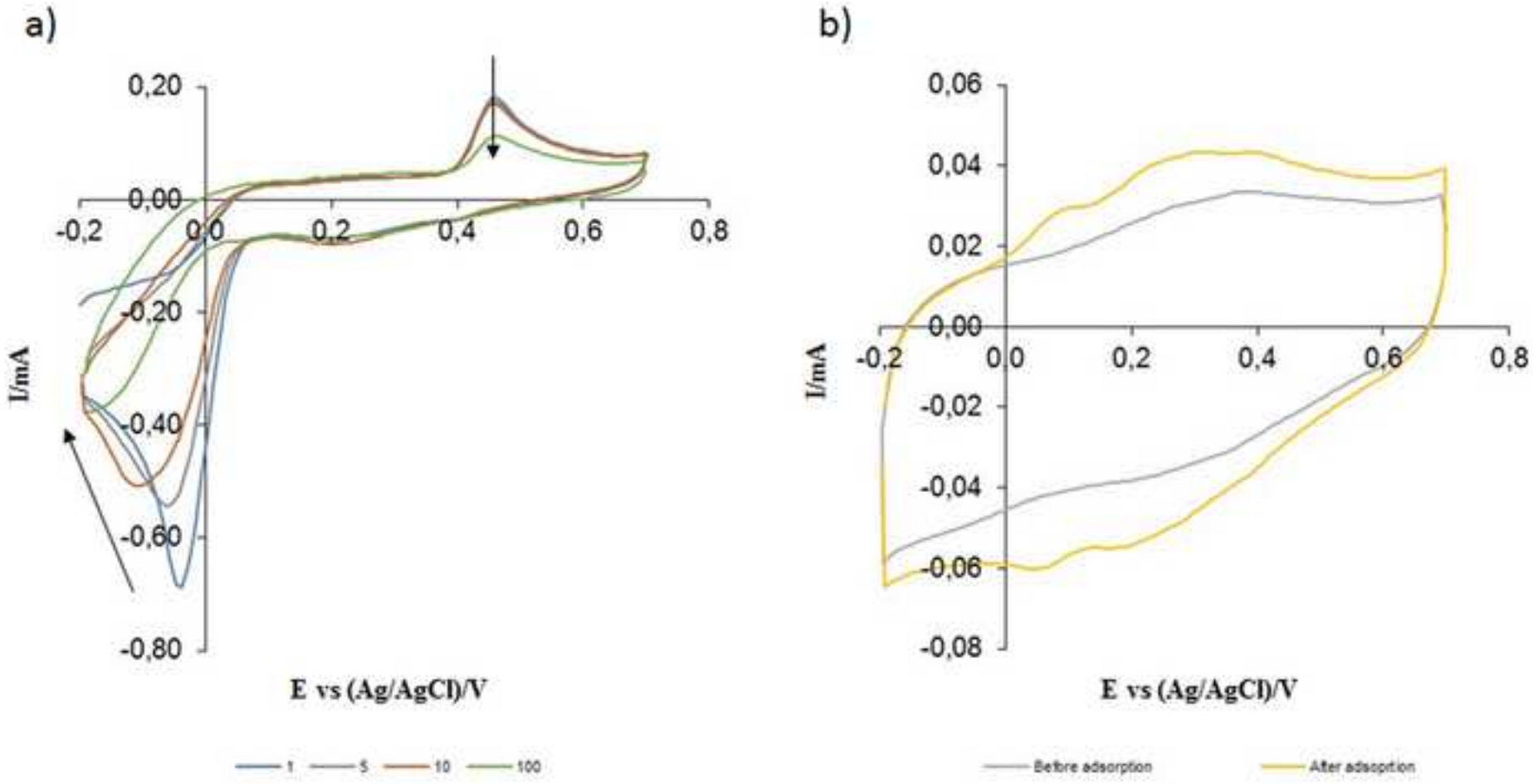

Table(1)

Table 1. Results of the fitting of impedance data of Pt and Pt/RGO electrodes in 0.5 M H_2SO_4. Data adjusted with the equivalent circuits shown in Fig. 3.

Electrode	Chi-Sqr	Rs (Ω)	CPE-T ($F^{CPE-P}.\Omega^{(1-CPE-P)}$)	CPE-P	Rct (Ω)
Pt	0,09	1,59	$1,72 \cdot 10^{-5}$	0,95	$1,77 \cdot 10^{5}$
Pt/RGO	0,02	2,03	$9,67 \cdot 10^{-4}$	0,87	-

Supplementary Materials

Click here to download Supplementary Materials: Supplementary Material.docx